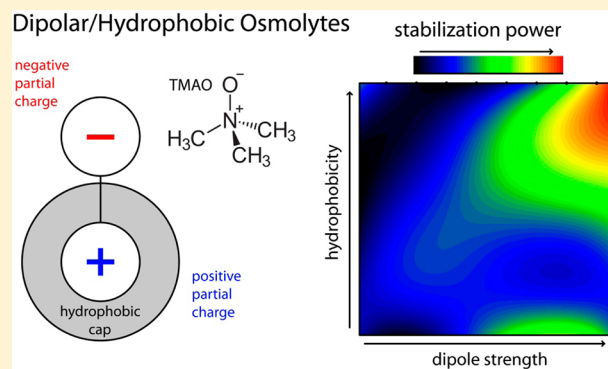


Insight into the Molecular Mechanisms of Protein Stabilizing Osmolytes from Global Force-Field Variations

Emanuel Schneck,^{†,‡,||} Dominik Horinek,^{‡,§} and Roland R. Netz*,^{†,‡}[†]Fachbereich Physik, Freie Universität Berlin, Arnimallee 14, 14195 Berlin, Germany[‡]Physik Department, Technische Universität München, 85748 Garching, Germany[§]Institut für Physikalische und Theoretische Chemie, Universität Regensburg, 93040 Regensburg, Germany

Supporting Information

ABSTRACT: A prominent class of osmolytes that are able to stabilize proteins in their native fold consist of small highly water-soluble molecules with a large dipole moment and hydrophobic groups attached to the positively charged end of the molecule, for which we coin the term dipolar/hydrophobic osmolytes. For TMAO, which is a prime member of this class, we perform large-scale water-explicit MD simulations and determine the bulk solution activity coefficient as well as the affinity to a stretched polyglycine chain for varying TMAO dipolar strength and hydrophobicity. Double optimization with respect to experimental values for the activity coefficient and the polyglycine transfer free energy is achieved. The resulting optimal TMAO force field shows excellent transferability to different concentrations and also reproduces transfer free energies of various amino acids, including the tryptophan anomaly, for which TMAO acts as a denaturant. By globally analyzing the thermodynamic and structural properties of suboptimal TMAO force fields, we identify the frustration between dipolar and hydrophobic interactions as the working mechanism and the design principle of dipolar/hydrophobic osmolytes.



INTRODUCTION

Stabilizing osmolytes are small, highly water-soluble molecules that thermodynamically favor the folded state of proteins over the unfolded one.¹ Nature uses them in all taxa in order to accommodate high external osmotic stresses² or to compensate the effects of denaturing agents such as urea.³ Naturally occurring stabilizers span a wide spectrum of chemical structures,⁴ ranging from methylated amino acids and methylamines, to ectoines,⁵ polyhydric alcohols such as sorbitol, and sugars such as sucrose and trehalose. Their ability to stabilize proteins in their native fold has been probed in numerous *in vitro* studies.^{6,7} Stabilization of folded proteins has traditionally been associated with a positive free energy difference for the transfer of the protein interior from water into osmolyte solution.^{8,9} Such transfer free energies (TFEs) have been extensively measured for different proteins, oligopeptides, and amino acids for all naturally occurring osmolytes.¹⁰

Early on, it was suggested⁸ and later confirmed^{11,12} that the TFE of short polypeptides can be expressed as the sum of the TFEs of their constituting amino acids. The TFEs of individual amino acids for denaturing as well as stabilizing cosolutes usually depend approximately linearly on the cosolute concentration,¹³ making the derivative of the TFE with respect to the cosolute concentration, denoted here as the *m*-value, a key quantity to assess and categorize cosolute effects. As follows directly from the Gibbs adsorption isotherm, the origin of

positive *m*-values (corresponding to positive TFEs and thus to protein folding stabilization) is the preferential exclusion of stabilizing osmolyte molecules from the peptide surface.¹⁴ Conversely, negative *m*-values coincide with preferential accumulation of denaturant molecules at the peptide surface.

MD simulations have immensely contributed to the understanding of osmolytic effects on protein stability.^{15–21} For the unfolding of entire proteins, the key problem is to estimate the degree to which osmolytes can interact with different chain sections along the unfolding pathway; in other words, detailed knowledge on the protein structure and conformation in the folded and unfolded ensemble is needed.^{9,17,22} However, even the much more basic question about the microscopic mechanism behind the repulsion between osmolyte molecules and a short peptide chain remained a subject of debate. Various stabilization mechanisms have been suggested, including molecular crowding,^{17,23} enthalpic effects,^{18,24,25} solvent structuring,^{16,19,20} and a competition between water–peptide, and solute–peptide interactions,^{15,18,26} but a comprehensive microscopic mechanism and in particular an explanation for the salient chemical structural features of common osmolytic stabilizers has not

Received: January 23, 2013

Revised: June 13, 2013

Published: June 15, 2013

been offered. Moreover, no atomistic simulation study has so far provided accurate predictions of *m*-values of polypeptides into osmolyte solutions, which would be a decisive check on the reliability of simulations and of any conclusions concerning molecular mechanisms drawn from such simulations.

We recently demonstrated for the test case of urea how to derive *m*-values from MD simulations and found reasonable agreement with experiments for a whole set of different amino acid residues if and only if suitably optimized force fields are used.²⁷ Here, we use the same simulation setup, involving a periodically replicated and stretched single peptide chain in an osmolyte solution of varying concentration, and study dipolar/hydrophobic osmolytes (DHOs). These chemical structures constitute a prominent class of stabilizing osmolytes, examples being the potent protein stabilizers TMAO and betaine, and loosely speaking consist of an extended dipole with hydrophobic groups attached around the positive part of the molecular dipole. In the past, the stabilizing effect of such osmolytes was explained in terms of the absence of polar groups that would strongly bind to the peptidic backbone,²⁶ unfavorable self-interactions,^{25,28} or repulsive steric interactions that would render the stabilizing akin to crowding effects.¹⁷ However, no theory tackled the question why a whole number of very efficient and naturally occurring stabilizing osmolytes combine dipoles with hydrophobic groups, two molecular properties that are antagonistic and separately would not yield any stabilizing property. We address this fundamental question by an approach that at first sight resembles global force-field optimization: we consider a large set of disperse TMAO force-field (ff) representations with widely varying dipole strength and hydrophobicity, effected by scanning the partial charges and the Lennard-Jones radius of the hydrophobic methyl groups, in this part we follow previous work of Garcia and co-workers.²⁵ For the entire set of TMAO ff's, we calculate both the TMAO solution activity coefficient, which is a sensitive measure of TMAO–TMAO interactions in bulk, as well as the effective interaction between TMAO molecules and a single polyglycine chain, from which the *m*-value can be derived. Both quantities are experimentally well-known and, by comparison between experimental data and our calculated values, our approach allows straightforward and simultaneous optimization of the TMAO ff by tuning the dipole moment and the hydrophobic strength.

However, it is not only the optimized ff we are after; rather, the suboptimal ff variants of TMAO are crucial for gaining insight into the mechanisms at work: Indeed, whereas a strong dipole moment or a pronounced hydrophobicity of TMAO by itself does not yield TMAO–peptide repulsion and thus stabilization of peptide folding, it is only the combination of these two molecular properties that leads to positive *m*-values in agreement with experimental numbers. The mechanism for this we identify to be the frustration of the dipolar interaction between TMAO and peptide dipoles due to the presence of the nearby hydrophobic groups, mediated by the strongly bound hydration water around TMAO. Interestingly, the combination of a pronounced dipole with sizable hydrophobic groups not only leads to peptide–TMAO repulsion but also to repulsion between TMAO molecules in bulk and therefore to an enhancement of the TMAO solution activity. Since the *m*-value is the product of the peptide–osmolyte repulsion and a factor that accounts for the concentration dependence of the bulk activity coefficient, this corresponds to a thermodynamic amplification of the stabilizing effect of TMAO, which might

explain the evolutionary success of stabilizing osmolytes based on the dipolar/hydrophobic design. The double optimization of the TMAO force field (ff) seems to be quite robust: Transferability is demonstrated by the good agreement with experimental *m*-values for different amino acids; in particular, our optimal ff reproduces the experimentally observed negative *m*-value of tryptophan, for which TMAO acts as a denaturant.

Our work demonstrates that, when insight into molecular mechanisms of naturally existing osmolytes is wanted, sometimes not much is gained by analyzing the ensemble of naturally existing structures, since they often result from harsh evolutionary selection and are subject to the strict boundary conditions of chemical feasibility and availability. Rather, deviations from such optimal designs, which in computer simulations are easily realized, even though they might not correspond to chemically realizable compounds, are essential for revealing the underlying molecular mechanisms.

METHODS

MD Simulations. For all simulations, we use the GROMACS package version 4.0,²⁹ SPC/E water³⁰ with SETTLE constraints for the water molecules,³¹ and LINKS restraints for other bonds involving hydrogen atoms.³² The simulation time step is $\Delta t = 2$ fs. The temperature is set to 300 K and controlled using the Nosé–Hoover thermostat³³ with a time constant of $\tau_T = 1$ ps. The pressure is set to 1 atm and controlled using the Parrinello–Rahman barostat³⁴ with a time constant of $\tau_p = 1$ ps and a compressibility parameter of $\kappa = 4.5 \times 10^{-10} \text{ Pa}^{-1}$, via isotropic or semi-isotropic pressure coupling for simulations of bulk solutions and simulations involving stretched peptides, respectively. The long-range electrostatics is treated by the smooth particle-mesh Ewald (PME) summation,^{35,36} with a real-space cutoff of 1.2 nm. A smooth van der Waals force cutoff is applied between 0.9 and 1.0 nm. Periodic boundary conditions (PBCs) are applied in all spatial directions. For polypeptides we use the amber94 ff,³⁷ for urea a Kirkwood–Buff optimized ff by Weerasinghe and Smith,³⁸ and for monomeric (i.e., zwitterionic) glycine we use bonded and Lennard-Jones parameters from the amber94 ff and partial charges generated using the RESP method.^{39,40} Our TMAO ff optimization started with the Kast parameters.⁴¹ For betaine, a ff was created on the basis of TMAO and glycine ff's: For all C-terminal atoms (CH_2 and COO^- groups), bonded and Lennard-Jones parameters as well as partial charges of the glycine ff were used. For all N-terminal atoms (CH_3 groups and N), bonded and Lennard-Jones parameters as well as partial charges of the Kast TMAO ff were used. In order to achieve charge neutrality of the betaine molecule, partial charges on N and C atoms of the N-terminus were adjusted by a negligible increment of ~ 0.01 e. Simulations of osmolyte bulk solutions have 100 ns duration and contain between 32 and 149 solute molecules in water in a simulation box of approximately $4 \times 4 \times 4 \text{ nm}^3$, resulting in mole fractions between $x_s = 0.015$ and $x_s = 0.090$. Solute–solute and solute–water radial distribution functions were computed after 20 ns of equilibration. Simulations of stretched peptides in solute solution have 100 ns duration and contain periodic deca-peptides aligned along the *z*-axis and extending through the entire simulation box. The first residue connects to the periodic image of the 10th and last residue in the adjacent periodic box. Thus, the system comprises a virtually infinite peptide chain, which has no terminal residues.²⁷ The length of the box in the *z*-direction is fixed at 3.6 nm during simulation and defines the average length

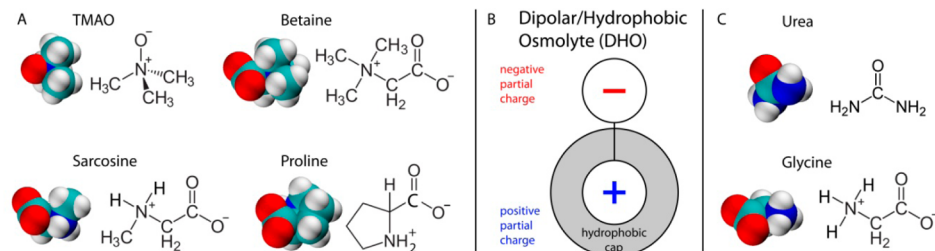


Figure 1. (A) Several examples of stabilizing dipolar/hydrophobic osmolytes (TMAO, betaine, sarcosine, and proline) and their chemical structures. (B) Simplified schematic drawing of a dipolar/hydrophobic osmolyte. (C) Chemical structures of the denaturant urea and glycine, which has only weak stabilizing power.

per residue, $l_{AA} = 0.36 \text{ nm}$. The box extension in the xy -direction is approximately $5 \times 5 \text{ nm}^2$. The remaining space of the box is filled with about 180 solute molecules in water, resulting in a mole fraction of $x_s \approx 0.1$.

Cylindrical radial distribution functions of solute and water molecules around the stretched peptide were computed after 50 ns of equilibration. Potentials of mean force (PMF) and interaction energies between two solute molecules as a function of their center of mass distance were extracted from umbrella sampling simulations of two solute molecules in bulk water kept at distances close to defined values between 0.3 and 1.3 nm in 15 steps using harmonic radial restraint potentials with spring constants between 1 and 20 MJ/(mol nm²). PMFs and interaction energies between one solute molecule and a stretched peptide were extracted from umbrella sampling simulations in an analogous way, with restraint potentials between the centers of mass of peptide and solute molecules in cylinder geometry. In order to minimize fluctuations in interaction energies, smaller simulation boxes were used in umbrella sampling simulations (bulk, approximately $3 \times 3 \times 3 \text{ nm}^3$; stretched peptides, $3.6 \text{ nm} \times$ approximately $3 \times 3 \text{ nm}^2$). Umbrella sampling simulations had durations $>160 \text{ ns}$ per distance. PMFs were then computed using the program g_wham.⁴² Ideal entropic centrifugal contributions were subtracted. Energies as a function of the radial separation in spherical or cylindrical geometries were extracted from the simulation output via energy/position correlation in the time domain. Entropic contributions were calculated as $-TS = G - H$.

Peptide *m*-Values and Enhancement Factors. The peptide TFE is defined as the change in free energy Υ per amino acid upon transfer of a stretched peptide from pure water into a solution with solute concentration c_s or solute mole fraction x_s . The degree of stretching was shown to have little influence on Υ .²⁷ The *m*-value is then the derivative of Υ with respect to c_s , expressed here in terms of the solute mole fraction x_s (see the Supporting Information for details):

$$m = \frac{d\Upsilon}{dc_s} = \frac{d\Upsilon}{dx_s} \frac{dx_s}{dc_s} \quad (1)$$

According to the Gibbs equation (see the Supporting Information for details), $d\Upsilon/dx_s$ can be expressed in terms of the preferential accumulation or exclusion of solutes from the stretched peptide, while the enhancement factor $(1 + f')$ takes into account nonideal solution effects:^{14,27}

$$\frac{d\Upsilon}{dx_s} = -k_B T \cdot l_{AA} \cdot \bar{\Gamma} \cdot (1 + f') \quad (2)$$

Here, k_B denotes the Boltzmann constant, T the temperature, $l_{AA} = 0.36 \text{ nm}$ the peptide length per amino acid, and the adsorption excess coefficient $\bar{\Gamma}$ is defined as

$$\bar{\Gamma} = \frac{\Gamma_s}{x_s} - \frac{\Gamma_w}{x_w} \quad (3)$$

where x_w denotes the water mole fraction and Γ_s and Γ_w the radial excesses per peptide unit length of solute and water molecules, respectively:

$$\Gamma_s = \int_0^\infty [g_s(r) - 1] 2\pi r dr \quad (4)$$

$$\Gamma_w = \int_0^\infty [g_w(r) - 1] 2\pi r dr \quad (5)$$

g_s and g_w denote the radial distribution functions in cylindrical coordinates of solute and water molecules, respectively, around the stretched peptide and are obtained in simulations of stretched peptides in aqueous solutions. The nonideality parameter f' denotes the logarithmic derivative of the bulk activity coefficient of the solute, f_s , with respect to the solute mole fraction x_s at constant temperature and pressure P

$$f' = \left(\frac{d \ln f_s}{d \ln x_s} \right)_{P,T} = - \frac{c_w x_s (K_{ss} + K_{ww} - 2K_{sw})}{1 + c_w x_s (K_{ss} + K_{ww} - 2K_{sw})} \quad (6)$$

where c_w denotes the water concentration. The connection to the solution structure is furnished by the Kirkwood–Buff integrals⁴³ over the normalized solute–solute, water–water, and solute–water radial distribution functions g_{ss} , g_{ww} , and g_{sw} in bulk:

$$K_{nm} = \int_0^\infty [g_{nm}(r) - 1] 4\pi r^2 dr, \quad \text{with } n, m \in \{s, w\} \quad (7)$$

We remark that K_{ww} drops out when the nonideality parameter on the molar concentration scale is calculated.³⁸

Peptide *m*-values at solute mole fractions of $x_s \approx 0.1$ (TMAO, $x_s = 0.08$; betaine, $x_s = 0.1$; glycine, $x_s = 0.08$; urea, $x_s = 0.08$) were calculated from adsorption excess coefficients $\bar{\Gamma}$ and enhancement factors $(1 + f')$ according to eqs 1 and 2. For this purpose, f' was computed in independent simulations of bulk solutions at similar concentrations (TMAO, $x_s = 0.08$; glycine, $x_s = 0.07$; urea, $x_s = 0.09$) as well as at other concentrations (see symbols in Figure 4A). For the calculation of peptide *m*-values in betaine solutions at $x_s = 0.1$, f' at $x_s = 0.1$ was extrapolated from f' at $x_s = 0.04$ under the approximation that f' depends linearly on x_s . As seen in the Supporting Information (Figure S1), this approximation is justified. In

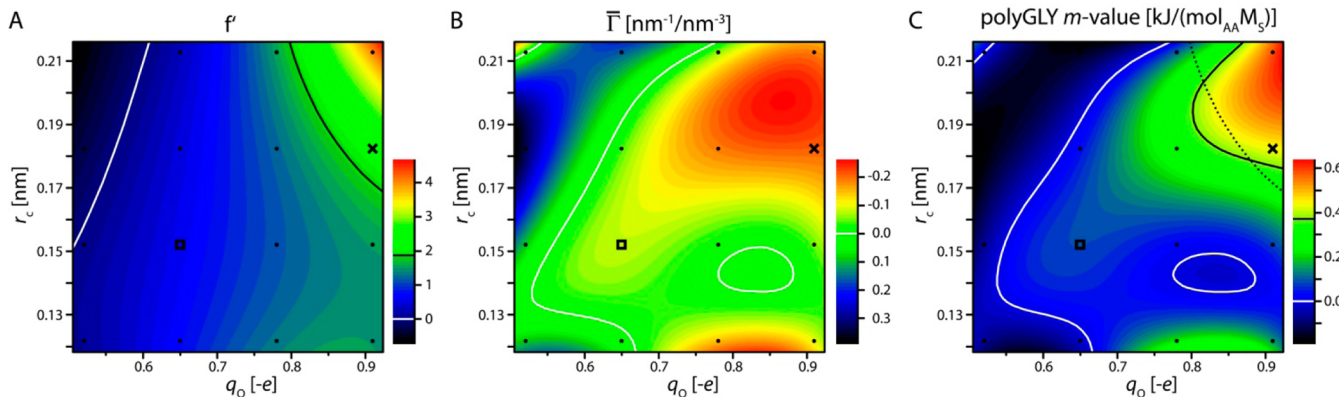


Figure 2. (A) TMAO nonideality parameter f' at a TMAO mole fraction of $x_s = 0.08$ as a function of oxygen partial charge q_O and methyl carbon radius r_c . The black line indicates the experimental value, $f' = 1.9$, derived from ref 44. The white line indicates ideal mixing behavior, i.e., $f' = 0$. (B) Adsorption excess coefficient $\bar{\Gamma}$ of TMAO at $x_s = 0.08$ as a function of the same parameters. White lines separate regions of stabilization ($\bar{\Gamma} < 0$) and denaturation ($\bar{\Gamma} > 0$) in the parameter space. (C) PolyGLY m -value as a function of the same parameters, calculated from (1 + f') and $\bar{\Gamma}$ according to eqs 1 and 2. The solid black line indicates the experimental value $m = 0.372 \text{ kJ}/(\text{mol}_{\text{AA}} \text{M}_S)$ taken from ref 45. The dotted black line corresponds to the experimental nonideality parameter shown as a solid black line in panel A. White lines separate regions of stabilization ($m > 0$) and denaturation ($m < 0$) in the parameter space. Black dots in each panel indicate parameter sets for which simulations were carried out. Color codes correspond to bicubic interpolation. Open squares indicate the Kast parameters, and crosses denote our optimized parameters.

order to facilitate direct comparison with experiments on their most common concentration scales, nonideality parameters were calculated on the mole fraction scale (see eq 6) and m -values on the molar concentration scale (see eq 1).

■ RESULTS AND DISCUSSION

The Paradigm of Dipolar/Hydrophobic Osmolytes. In this paper, we focus on a class of osmolytes that we denote as *dipolar/hydrophobic osmolytes* (DHOs). The potent protein stabilizers TMAO and betaine but also the slightly less efficient stabilizers sarcosine and proline belong to this class, which is characterized by a strong electrical dipole with the positive charge capped or shielded by hydrophobic methyl groups.

Figure 1 presents chemical structures of various osmolytes. Panel A shows the DHOs TMAO, betaine, sarcosine, and proline. Panel B shows a simplified schematic drawing of a DHO. For comparison and contrast, the denaturant urea and glycine (which is halfway between stabilizing and denaturing) are shown in panel C. It is seen that the division between denaturants and stabilizers is diffuse: Glycine is turned into a stabilizing agent by gradually adding one (sarcosine) to three (betaine) methyl groups to the cationic part. On the other hand, the structural differences between urea, a common denaturant, and TMAO, one of the most potent stabilizers, are not dramatic. It transpires that, to unveil the working principles of DHOs, quantitative analysis is needed.

Mechanistic Insight from Force-Field Optimization of TMAO. TMAO is the structurally simplest naturally occurring DHO and also one of the most potent known protein stabilizers. We therefore study TMAO in detail and only report sparse results on other DHOs. To explore the role of the two key features of DHOs, dipolarity and hydrophobicity, we systematically vary TMAO's dipole strength and hydrophobic group size and monitor the influence on the TMAO bulk solution behavior and its peptide affinity.

All bonded parameters (i.e., potentials for bond lengths, angles, and dihedrals), Lennard-Jones (LJ) parameters of oxygen (O) and nitrogen (N) atoms, and partial charges of methyl carbon (C) and hydrogen (H) atoms were adopted from the Kast TMAO ff⁴¹ and not modified (see Tables S1a–

S1d, Supporting Information). Intramolecular non-bonded 1–4 interactions were treated with the pre-factors dictated by the amber94 ff (0.5 for LJ and 0.83 for Coulomb interactions) and thus differently than foreseen by Kast et al. (1 for LJ and 0 for Coulomb interactions). The ensuing differences can be assumed to have no influence on the conclusions drawn below. Small variations in the bond lengths, for instance, do not have a significant influence on the observed trends, as shown in the Supporting Information. To tune the TMAO dipole strength, the partial charge of O is varied in steps between $q_O = -0.52 \text{ e}$ and $q_O = -3 \text{ e}$, where e denotes the elementary charge, and the partial charge of N is adjusted such that TMAO as a whole remains neutral. The size of the methyl groups around the positive charge and thereby their hydrophobicity is tuned by systematic variation of the Lennard-Jones radii r_C and r_H of methyl C and H atoms at fixed ratio r_C/r_H and fixed Lennard-Jones energy ϵ . r_C is varied from $r_C = 0.12 \text{ nm}$ to $r_C = 0.21 \text{ nm}$.

Panels A and B of Figure 2 show the nonideality parameter f' and the adsorption excess coefficient $\bar{\Gamma}$ at a polyGLY chain at TMAO concentration $x_s = 0.08$ as a function of q_O (representing the dipole strength) and r_C (representing the hydrophobicity). Panel C shows the polyGLY m -value calculated according to eqs 1 and 2. Black dots in panels A, B, and C indicate the 16 parameter combinations for which simulations were carried out: $q_O \in \{-0.52 \text{ e}, -0.65 \text{ e}, -0.78 \text{ e}, -0.91 \text{ e}\}$ and $r_C \in \{0.12 \text{ nm}, 0.15 \text{ nm}, 0.18 \text{ nm}, 0.21 \text{ nm}\}$. Color codes represent bicubic interpolations (see the Supporting Information for details) in the parameter space shown. Open squares indicate the parameter set ($q_O = -0.65 \text{ e}$ and $r_C = 0.15 \text{ nm}$) of the Kast ff. A negative nonideality parameter in Figure 2A ($f' < 0$) corresponds to attraction between the TMAO molecules in bulk solution, and positive values ($f' > 0$) correspond to repulsion. The white line indicates ideal behavior ($f' = 0$). f' exhibits smooth parameter dependence with systematic trends: For weak electric dipole (to the left), f' decreases with increasing hydrophobicity, which is expected and reflects enhanced hydrophobic attraction between TMAO molecules. For strong electric dipoles (to the right), on the other hand, f' increases as one goes up in the

diagram, and we obtain the—at first sight puzzling—result that increasing hydrophobicity leads to enhanced repulsion between TMAO molecules. This finding lies at the heart of the DHO mechanism and will be discussed from different angles in detail in this paper. It is instructive to also consider horizontal paths in the diagram in Figure 2A: we find that f' exhibits only weak dependence on the dipole strength for small hydrophobicity (at the bottom), while it strongly increases with increasing dipole strength for large methyl groups (at the top). This means that the repulsion between two TMAO molecules increases as their dipole moments go up, in contrast to the contrary naïve expectation based on the fact that freely orientable dipoles in a vacuum attract each other in direct proportion to their dipolar strength. To reconcile these perplexing results with standard electrostatics, we show in Figure 3 the enhancement factor ($1 + f'$)

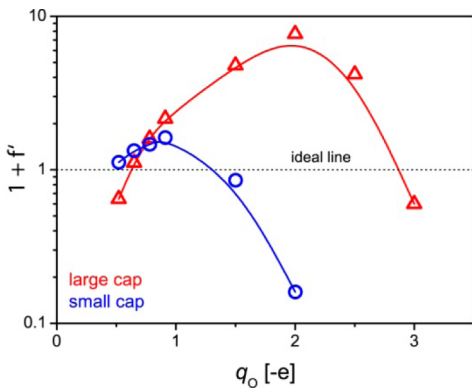


Figure 3. TMAO enhancement factor ($1 + f'$) at a mole fraction of $x_s = 0.03$ for small ($r_C = 0.12 \text{ nm}$, blue circles) and large ($r_C = 0.21 \text{ nm}$, red triangles) hydrophobic groups as a function of the dipole strength. Note that the turnover and the attractive regime, characterized by $(1 + f') < 1$, are only obtained for unrealistically high dipole strengths. Solid lines are guides to the eye.

f') at a TMAO mole fraction of $x_s = 0.03$ as a function of a wide range of dipole strengths for small ($r_C = 0.12 \text{ nm}$, circles) and large ($r_C = 0.21 \text{ nm}$, triangles) methyl radii. Note that in this plot we show results for oxygen partial charges up to unrealistically high values of $q_O = -3 \text{ e}$. In agreement with the contour plots shown in Figure 2A, $(1 + f')$ first increases with increasing dipole strength but then turns over. For large

methyl group size $r_C = 0.21 \text{ nm}$, we reach enormously high values ($1 + f' = 8$) for charges of $q_O \approx -2 \text{ e}$, corresponding to remarkably strong repulsion between the highly dipolar TMAO variants, but eventually, for partial charges beyond $q_O \approx -2.8 \text{ e}$, the bare dipole–dipole interaction between TMAO molecules takes over and the enhancement factor drops below unity, indicative of net attraction between TMAO molecules. For small hydrophobicity, the maximum in $(1 + f')$ is much smaller and occurs at significantly lower partial charges. This indicates that it is mainly the hydrophobic groups around the positive molecular charge that prevent electrostatically favorable relative orientations of the TMAO dipoles in an aqueous environment for all realistic values of partial charges. This dipolar/hydrophobic frustration mechanism is further detailed below on the basis of a decomposition analysis of the Gibbs free energy of interaction between two TMAO molecules. Coming back to the contour plot in Figure 2A, the experimental value $f' = 1.9$, derived from ref 44 and indicated by a black line, is only reproduced for a TMAO ff that combines a large dipole moment with pronounced hydrophobicity (in the upper right corner).

The adsorption excess coefficient $\bar{\Gamma}$ for TMAO at a polyGLY chain in Figure 2B exhibits a slightly more complex parameter dependence but roughly follows the same trends: Pronounced preferential exclusion of TMAO from a polyGLY chain ($\bar{\Gamma} < 0$), corresponding to protein stabilization, is only observed for high dipole strengths in conjunction with pronounced hydrophobicity, i.e., in the upper right corner. White lines indicate neutral behavior at which the excess vanishes identically ($\bar{\Gamma} = 0$).

The polyGLY m -value in Figure 2C follows from the product of $(1 + f')$ and $\bar{\Gamma}$ according to eq 2. White lines indicate neutral behavior ($m = 0$), while the solid black line denotes the experimental m -value. Graphical inspection of Figure 2A and C shows that the experimental nonideality parameter f' and m -value can be simultaneously reproduced in the upper right corner of the ff diagram, i.e., for large dipole strength and sufficiently large hydrophobic methyl group size. The dotted black line once again indicates the parameter sets that yield the experimental nonideality parameter and is copied from Figure 2A. The best-matching parameter set for which simulations were carried out, $q_O = -0.91 \text{ e}$ and $r_C = 0.18 \text{ nm}$, denoted by a cross in Figure 2 yields good simultaneous agreement for the enhancement factor (experiment, 2.9; simulation, 3.0) as well as

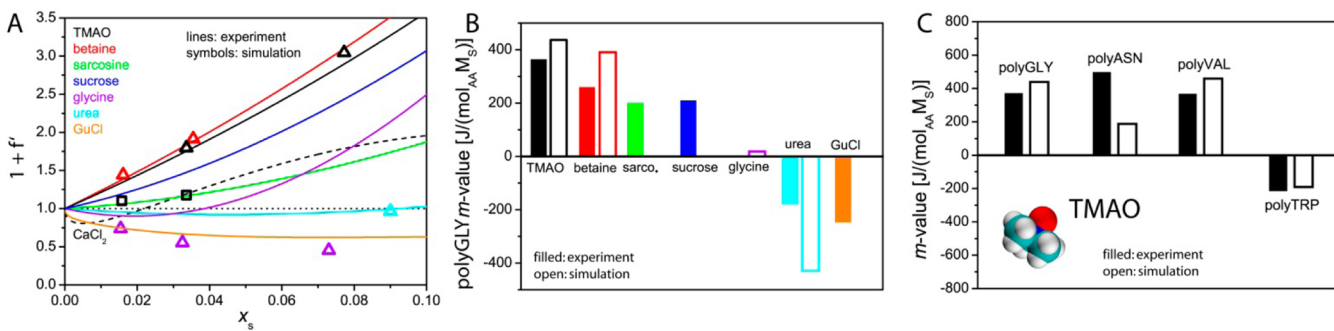


Figure 4. (A) Enhancement factors ($1 + f'$) of various solutes (TMAO, betaine, sucrose, sarcosine, glycine, urea, guanidinium chloride (GuCl), and CaCl_2) as a function of the solute mole fraction x_s . Solid lines indicate experimental values derived from refs 44 and 46–48. Symbols indicate our simulation results obtained for various solutes. Squares correspond to the Kast parameters.⁴¹ The dotted horizontal line indicates ideal mixing behavior ($f' = 0$). (B) Polyglycine m -values for various solutes. Filled columns indicate experimental values taken from refs 11 and 26. Open columns indicate our simulation results. (C) TMAO m -values for various homopolypeptides (polyGLY, polyASN, polyVAL, and polyTRP). Filled columns indicate experimental values taken from ref 45. Open columns indicate our simulation results.

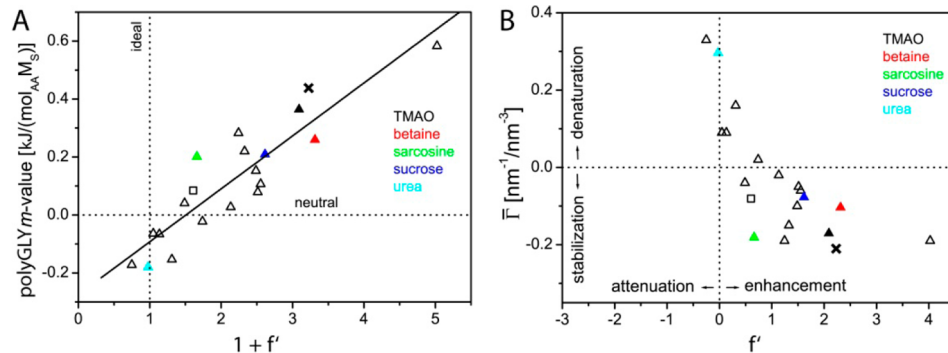


Figure 5. (A) PolyGLY m -values for various solutes plotted versus enhancement factor ($1 + f'$) at $x_s = 0.08$. Experimental data points are shown as filled triangles. Those obtained in our MD simulations with various TMAO force-field variants are shown as open triangles. Open square: Kast ff. Cross: Our optimized ff. Solid line: linear fit through all data points. (B) Excess coefficient $\bar{\Gamma}$ plotted versus f' for the same data set. This representation allows one to separately distinguish between stabilizing and denaturing osmolytes on the one hand and attenuating and enhancing bulk solution effects on the other hand.

for the polyGLY m -value (experiment,⁴⁵ 372 J/(mol_{AA}M_S); simulation, 438 J/(mol_{AA}M_S)). It should be noted that these parameters correspond to a thermodynamic optimization within the framework of atomistic molecular dynamics simulations, employing a significantly simplified treatment of molecular interactions. The obtained TMAO parameters thus are affected by the limitations of the water and peptide models, the assumption of pairwise additive potentials, etc., and therefore deviate from parameters determined in quantum chemical approaches or crystallographic optimization. The TMAO ff by Kast et al.,⁴¹ for instance, was mainly optimized with respect to crystallographic and spectroscopic information, while our TMAO ff is optimized with respect to solution activity and glycine m -values, and also reproduces the density of aqueous TMAO solutions quite well (see Figure S2 in the Supporting Information). However, these restrictions, inherent to MD simulations and heuristic ff's in general, should not impair the more general conclusions drawn in the present study. In the following, we will benchmark our optimized TMAO ff with experimental TFE data for different amino acids but will also analyze results for less optimal TMAO ff parameters in order to gain insight into the mechanisms and the common features of DHOs.

Benchmarking with Experimental Data. Figure 4A shows experimental enhancement factors ($1 + f'$) (solid lines) for various stabilizing osmolytes (TMAO, betaine, sarcosine, sucrose, and glycine), two denaturants (urea and guanidinium chloride (GuCl)), and the electrolyte CaCl₂ as a function of the solute mole fraction x_s , derived from refs 44 and 46–48. With the well-known exception of urea, the experimental values for ($1 + f'$) substantially deviate from unity, reflecting pronounced nonideal mixing. This is particularly important for the stabilizing effect of osmolytes, since, according to eq 2, the enhancement factor ($1 + f'$) strongly influences peptide m -values. Symbols in Figure 4A indicate our MD simulation results. For TMAO, betaine, and urea, we find excellent quantitative agreement between simulation and experiment (note that squares indicate our simulation results obtained with the Kast parameters, $q_0 = -0.65 \text{ e}$ and $r_c = 0.15 \text{ nm}$).⁴¹ For TMAO and urea, this agreement is expected, since we use ff's optimized to correctly reproduce the solution thermodynamics; for urea, this was done in ref 38, and for TMAO, this is done in the present study. We note that the good agreement over a wide

concentration range shows that the ff optimization is quite robust for urea and TMAO. For betaine, for which no systematic optimization was pursued, the agreement is still remarkable, and for glycine, sizable deviations are noticed. Most strikingly, TMAO and betaine exhibit very high enhancement factors, reflecting considerable self-repulsion in bulk and thus pronounced amplification of m -values due to eq 2. The tendency of many osmolytes to exhibit strongly nonideal mixing behavior has been correlated with hydration effects;²⁸ in this paper, we reveal the more detailed dipolar/hydrophobic frustration mechanism as the basis for this trend.

Figure 4B shows polyglycine m -values for various osmolytes. Experimental values (filled columns) are taken from Auton et al.¹¹ and Street et al.²⁶ Simulation results are denoted by open columns and follow from eqs 1 and 2 obtained at $x_s \approx 0.1$ (TMAO, $x_s = 0.08$; betaine, $x_s = 0.1$; glycine, $x_s = 0.08$; urea, $x_s = 0.08$). The corresponding data are shown side by side if both are available for the same solute. Experimentally, the osmolytes TMAO, betaine, sarcosine, and sucrose exhibit large positive polyglycine m -values. This reflects strong preferential exclusion from the backbone and indicates strong stabilization of polypeptides in their folded configuration, which is characterized by a relatively smaller solvent-exposed surface area. Urea and guanidinium chloride (GuCl), in contrast, exhibit negative m -values of comparable magnitude, reflecting preferential enrichment at the peptide backbone and thus destabilization of folded peptide configurations. MD simulation results for TMAO, betaine, and urea are fully consistent with this trend. The solute glycine, for which no experimental value is available, shows an almost neutral behavior, with an only slightly positive m -value corresponding to weak protein stabilization (which is surprising in light of the significant experimental stabilization of ribonuclease A and lysozyme by glycine⁶). Due to the only moderate nonideality of glycine's mixing behavior, its m -value is rather directly linked to the surface excess, as in the case of urea, and in contrast to most stabilizing osmolytes.⁴⁹ The clear trend when comparing glycine with sarcosine and betaine is that the m -value increases strongly and monotonically as more methyl groups are added to the positively charged end of the molecule.

Figure 4C compares experimental⁴⁵ and our simulation TMAO m -values for various polypeptides. One notes that m -values differ significantly between different amino acids. Polyglycine (polyGLY), polyasparagine (polyASN), and

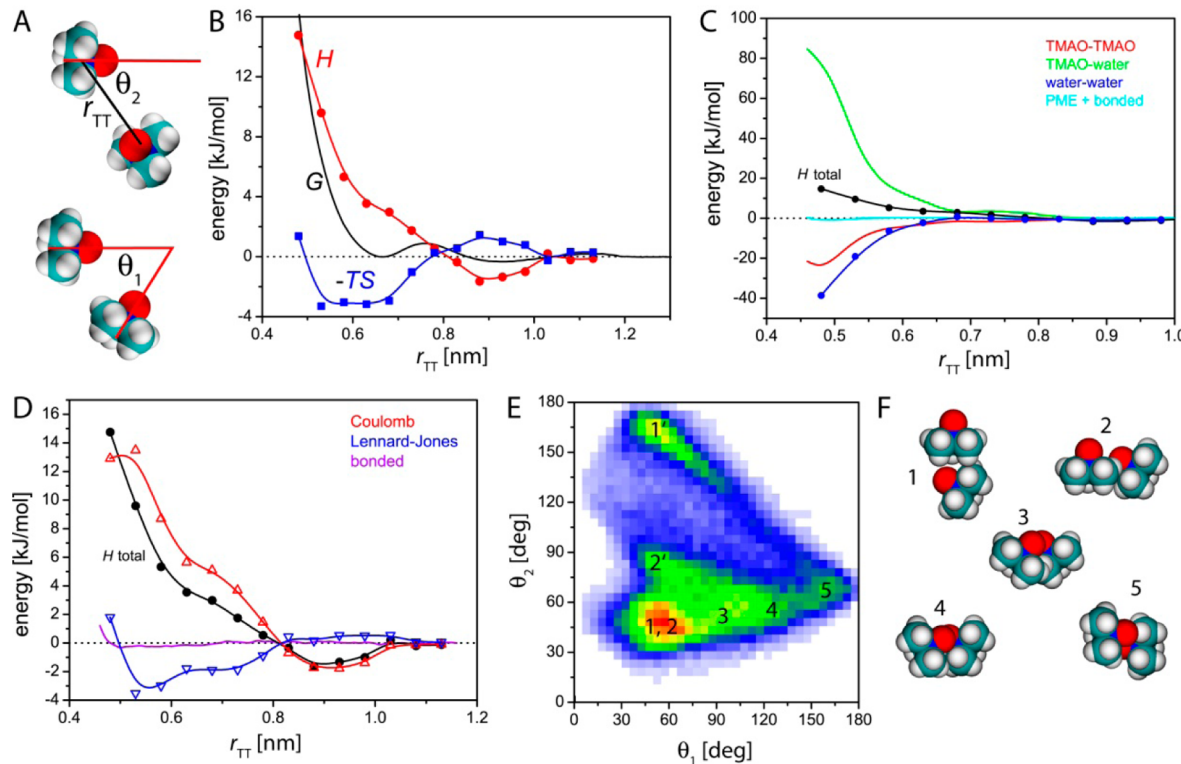


Figure 6. (A) Snapshots of two TMAO molecules at a center of mass distance r_{TT} and relative orientations measured by the angles θ_1 (between the dipole vectors) and θ_2 (between dipole and center-of-mass connecting vectors). (B) Interaction free energy G of two near-optimal TMAO molecules with strong dipole ($q_O = -0.91 e$) and large hydrophobicity ($r_C = 0.21 \text{ nm}$) and the enthalpic (H) and entropic ($-TS$) contributions, all as a function of the TMAO–TMAO distance r_{TT} . Solid lines are guides to the eye. (C) Decomposition of the interaction enthalpy H into molecular pair potentials (TMAO–TMAO, TMAO–water, and water–water), bonded, and long-range electrostatic (PME) potentials. (D) Decomposition of H into electrostatic, Lenard-Jones, and bonded contributions. (E) Distribution of the angles θ_1 and θ_2 (as defined in panel A) at a center-of-mass distance of $r_{TT} = 0.52 \pm 0.01 \text{ nm}$, exhibiting several maxima corresponding to five different relative orientations of the TMAO molecules denoted with 1, 2, 3, 4, and 5. (F) Schematic drawing of the dominant relative orientations.

polyvaline (polyVAL) have large and positive m -values, while that of polytryptophan is negative with almost comparable magnitude. There is no obvious correlation between size or polarity of the side chains and the corresponding TMAO m -values. This is in contrast to the denaturant urea for which m -values are found to roughly scale with the size of the side chains.²⁷ Although the simulations fail to correctly predict the large m -value of polyASN, they reproduce the qualitative experimental trends. This is remarkable, since the TMAO ff optimization was done with polyglycine only, and shows that the optimized ff is transferable to other situations than it was optimized for. Deviations have to be attributed to remaining ff limitations of the amino acids. As shown in the Supporting Information (Figure S2), our optimization also improves the agreement of the TMAO solution density with experiments.

Toward a Global Phase Diagram of Dipolar/Hydrophobic Osmolytes. In Figure 5A, polyGLY m -values are plotted versus the enhancement factor ($1 + f'$) at fixed concentration $x_s = 0.08$ for various solutes. Filled triangles indicate experimental values derived from refs 44 and 47, while open triangles indicate simulation results for all ff representations of TMAO with nonoptimal parameter combinations. The open square indicates the Kast parameters, and the cross, our optimized parameters. A linear correlation between m -values and enhancement factors has been recognized previously based on experimental data for a whole set of osmolytes.²⁸ The solid line in Figure 5A is a linear fit through all data points and shows that the correlation exists also for all different chemical

architectures represented by the variants of TMAO-based ff's considered by us. However, a look at eq 2 shows that such a linear correlation would be expected already for a constant adsorption excess coefficient $\bar{\Gamma}$ and is per se not surprising or revealing.

A more meaningful comparison is presented in Figure 5B, where $\bar{\Gamma}$ for polyGLY is plotted versus the nonideality parameter f' for the same data set. Experimental values of $\bar{\Gamma}$ (filled triangles) are deduced from the experimental enhancement factors and m -values via inversion of eq 2. The corresponding correction factors dx_s/dc_s are approximated from the experimental molecular volumes reported in refs 38 and 50–52, as described in the Supporting Information. Figure 5B clearly distinguishes “stabilizers”, characterized by $\bar{\Gamma} < 0$ and located in the lower half, from “denaturants”, characterized by $\bar{\Gamma} > 0$, located in the upper half. The horizontal axis distinguishes solutes with $f' < 0$, located to the left, which attract each other in bulk solution and for which the m -value is attenuated according to eq 1, from solutes with $f' > 0$, located to the right, which repel each other in bulk and for which the m -value is enhanced. Quite surprisingly, all TMAO force-field variants considered by us, which differ in dipole strength as well as hydrophobicity, lie on a broadly defined master curve, which suggests that it is a single effective osmolyte property that controls both osmolyte self-interactions (embodied in f') as well as polyGLY–osmolyte interactions (embodied in $\bar{\Gamma}$). This fact points to a common mechanism responsible for the repulsion between DHOs as well as for the repulsion between

polypeptides and DHOs, as will be explained further below. Interestingly, some of the TMAO ff variants considered by us are in fact denaturants, characterized by $\bar{\Gamma} > 0$ and consequently negative m -values, while the nonideality parameters are basically all positive ($f' > 0$), indicating net repulsion between osmolytes in bulk (we remark that the drastically modified ff sets from Figure 3 which exhibit attraction between TMAO in bulk are not included in this graph).

We conclude that, with a generic dipolar/hydrophobic design as studied by us, a gradual transition between stabilizing and denaturing osmolytes is achieved. While basically no ff variant exhibits pronounced attraction in bulk, characterized by $f' < 0$ (and which eventually would render the bulk solution unstable), stabilizing osmolytes ($\bar{\Gamma} < 0$) tend to be highly efficient, since the positive enhancement factor ($f' > 0$) amplifies the m -value. On the other hand, denaturing ff variants (characterized by $\bar{\Gamma} > 0$) are only modestly efficient, since they have a close-to-vanishing value of f' . This again reflects that the dipolar/hydrophobic frustration mechanism that leads to repulsion between TMAO molecules is the same mechanism that leads to repulsion between TMAO and polyGLY.

TMAO–TMAO Interaction in Detail. According to eqs 6 and 7, the nonideality parameter f' follows from the solute–solute, water–water, and solute–water radial distribution functions g_{ss} , g_{ww} and g_{sw} which themselves are determined by the potentials of mean force (PMF) between two solute molecules, two solvent molecules, and between a solute and a solvent molecule, respectively. $f' > 0$ corresponds to unfavorable solute–solute and solvent–solvent interactions compared to the solute–water interaction. Since this interplay is mostly dominated by the effective TMAO–TMAO interaction (as shown in Figure S3 in the Supporting Information), we in Figure 6 analyze in detail the interaction between two TMAO molecules with near-optimal ff parameters, i.e., a strong dipole ($q_0 = -0.91\text{ e}$) and large hydrophobicity ($r_C = 0.21\text{ nm}$) in bulk water.

Figure 6A shows snapshots of two TMAO molecules at a center of mass distance r_{TT} and defines the relative angles θ_1 and θ_2 that are used later on. Figure 6B shows the PMF (i.e., the interaction free energy G as a function of r_{TT}) between two TMAO molecules in bulk water (solid black line). The non-monotonic shape reflects the discrete hydration layers which are sequentially stripped off as the two TMAO molecules approach each other. Despite weak local minima, G is strongly repulsive at short distances. The separation into enthalpic (H , red data points) and entropic ($-TS$, blue data points) contributions shows that the repulsion at short distances ($r_{TT} < 0.8\text{ nm}$) is of enthalpic origin, while the entropy is attractive in this distance range. This suggests that the repulsion is not of steric or excluded volume origin, in which case the repulsion should be dominated by entropy. For TMAO with low partial charges ($q_0 = -0.52\text{ e}$), we find the entropic attraction to overwhelm the enthalpic repulsion (see Figure S4A in the Supporting Information), in agreement with the negative nonideality parameters ($f' < 0$) in Figure 2A, while, for TMAO with small hydrophobic groups, entropic attraction is much less pronounced (see Figure S5A in the Supporting Information). Both observations indicate that the entropic attraction mainly reflects nonpolar interactions and is related to the hydrophobic effect.⁵³ We remark that this conclusion cannot be drawn without ff variations, since opposite charges in water also experience entropic attraction due to the pronounced temperature dependence of the dielectric constant

of water. Therefore, the presence of entropic attraction alone is not necessarily indicative of hydrophobic effects.⁵⁴

The further decomposition of the enthalpy H into TMAO–TMAO, TMAO–water, and water–water pair-contributions in Figure 6C demonstrates that the TMAO–TMAO repulsion is solely due to water–TMAO interactions. In other words, when two TMAO molecules approach each other, they have to strip off strongly bound hydration water, which costs enthalpy. The resulting effect resembles steric repulsion in a superficial sense, if TMAO molecules in conjunction with their hydration shells are interpreted to act like effective steric quasiparticles. One notes, however, that the thermodynamics is enthalpy dominated and thus very different from excluded volume effects, so the merit of such a steric picture is doubtful. It transpires that simple models, which neglect the role of hydration water around osmolytes, will be entirely inadequate for the description of DHO behavior.

More insight into the enthalpic repulsion in Figure 6B can be gained from a different decomposition of the enthalpy, into Lennard-Jones and electrostatic contributions. As shown in Figure 6D, the enthalpic repulsion between TMAO molecules in water is driven by electrostatics, while bonded interactions play no significant role and Lennard-Jones interactions (accounting for both vdW attraction and short-ranged repulsion) are even slightly attractive. This indicates that the break-up of the TMAO hydration layers at short separations, seen in Figure 6C, mostly results in an electrostatic enthalpy penalty. The remarkable feature of DHOs is that this enthalpy penalty is linked with the presence of large hydrophobic groups; in fact, this electrostatic repulsion becomes much weaker for smaller hydrophobicity (see Figure SSC in the Supporting Information).

An equivalent observation is that the hydrophobic groups around the positive charge prevent the TMAO molecules from assuming favorable relative dipole orientations. Figure 6E shows probability distributions in the plane spanned by the two relative angles θ_1 and θ_2 , defined in Figure 6A, at a center of mass distance of $r_{TT} = 0.52\text{ nm}$, where significant repulsion takes place ($G \approx 10\text{ kJ/mol} \approx 4 k_B T$, see panel B). The angular distribution exhibits several local maxima denoted as 1–5, and schematically depicted in Figure 6F. In all depicted configurations, except for the only weakly occupied configuration 5, the hydrophobic groups around the positive charges are in contact, consistent with the interpretation of the minimum in the entropic term at about the same distance $r_{TT} = 0.52\text{ nm}$ as being caused by hydrophobic attraction. In all depicted configurations, TMAO molecules are prevented from assuming relative orientations that would minimize the dipole–dipole interaction (see also Figure S6 in the Supporting Information), which is thus traced back to the presence of bulky hydrophobic groups. It is this interplay of dipolar effects (which lead to a strongly bound hydration shell and thus electrostatic enthalpic repulsion between two TMAO molecules) and hydrophobic effects (which give rise to weak entropic attraction between TMAO molecules but at the same time prevent two TMAO molecules to take on configurations that would lead to strong dipolar attraction) which we argue to be at the core of the working principle of DHOs and which we call the dipolar/hydrophobic frustration mechanism.

TMAO–Polyglycine Interaction. Large positive polyGLY m -values reflect unfavorable interactions between TMAO and the stretched polyGLY chain, in analogy to the scenario of two TMAO molecules discussed above. Figure 7A shows snapshots

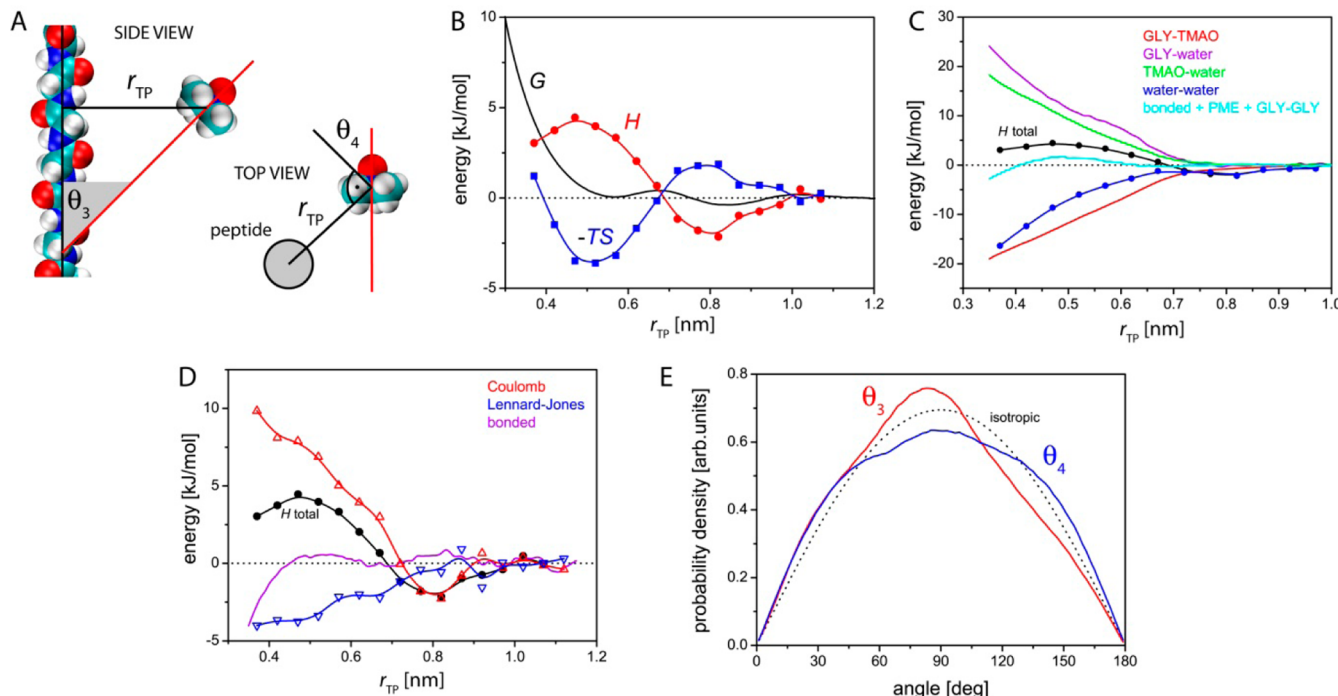


Figure 7. (A) Snapshots (side view and top view) of a TMAO molecule at a center-of-mass distance r_{TP} from a stretched polyGLY chain in water (water molecules are not shown). The orientation of TMAO with respect to the polyGLY is defined by the angles θ_3 and θ_4 . (B) Interaction free energy G between a TMAO molecule with strong dipole ($q_O = -0.91 e$) and large hydrophobic cap ($r_C = 0.21 \text{ nm}$) and polyGLY, plotted together with the enthalpic (H) and entropic ($-TS$) contributions, all as a function of the TMAO-peptide distance r_{TP} . (C) Decomposition of the interaction enthalpy H into molecular pair potentials (peptide-TMAO, peptide-water, TMAO-water, water-water, and peptide-peptide), bonded, and long-range electrostatic (PME) potentials. (D) Decomposition of H into electrostatic, Lennard-Jones, and bonded contributions. (E) Distribution of the angles θ_3 and θ_4 (as defined in panel A) at a center-of-mass distance of $r_{TP} = 0.38 \pm 0.01 \text{ nm}$. The broken black line indicates distributions expected in the case of orientational isotropy.

(side view and top view) of a TMAO molecule at a cylindrical center of mass distance r_{TP} from a stretched polyGLY chain. Figure 7B shows the potential of mean force G between the TMAO molecule with strong dipole ($q_O = -0.91 e$) and large hydrophobicity ($r_C = 0.21 \text{ nm}$) and polyGLY as a function of r_{TP} (solid black line). The behavior is similar to the TMAO-TMAO case: For short distances, G is repulsive, consistent with the large negative $\bar{\Gamma}$ values obtained for similar TMAO parameters in Figure 2B. For short distances ($r_{TP} < 0.7 \text{ nm}$), the entropic contribution (blue data points) is strongly favorable, while the enthalpy (red data points) is unfavorable and dominant. This observation is consistent with experiments by Zou et al. that showed the positive polyGLY m -value of TMAO to have a strong positive enthalpic contribution that overcompensates a negative entropic term of comparable magnitude.²⁰ In fact, enthalpy-driven stabilization has also been identified for various other cosolutes.^{24,55} As seen in Figure S7 of the Supporting Information, for significant entropic attraction, it is required that TMAO molecules possess sufficiently large hydrophobic groups, which also points toward an important (albeit antagonistic) role of the hydrophobic effect in protein stabilization by DHOs. The importance of nonpolar interactions has been recognized in the case of protein denaturants⁵⁶ but has been vastly neglected in the context of stabilizing osmolytes so far. In fact, although polyGLY has strong partial charges located at N, O, and carbonyl C atoms, nonpolar moieties (formed by C_α and H atoms) are solvent-exposed as well and therefore significant hydrophobic contributions are expected. The interaction enthalpy profile $H(r_{TP})$ is the result of a complex interplay

between polyGLY-TMAO, polyGLY-water, TMAO-water, and water-water pair contributions, as shown in Figure 7C. In addition, intra-polyGLY bonded and nonbonded interactions as well as long-range electrostatics (PME, see the Methods section) play small roles.

As in the case of TMAO-TMAO interactions, water effects dominate. The importance of the hydration of TMAO and polyGLY molecules during interaction has previously been identified and investigated on a structural level.⁵⁷ The near-cancellation of TMAO-water (green) and water-water (blue) pair interactions might help rationalize the success of theoretical models that neglect water-water and solute-water interactions in this balance.²⁶ As shown in Figure 7D, the resulting enthalpic repulsion between TMAO and polyGLY in water is driven by electrostatics overwhelming attractive vdW and bonded interactions. The same qualitative result was obtained in a previous MD simulation study on the TMAO/polyGLY interaction, despite considerable differences in force fields and methodology.¹² The interplay between electrostatic repulsion and subdominant hydrophobic attraction is again attributed to the dipolar/hydrophobic frustration mechanism (as shown in Figure S7 in the Supporting Information, for small hydrophobic caps the repulsion is much weaker), similar to the interaction between two TMAO molecules discussed before. Figure 7E shows distributions of relative angles between TMAO and polyGLY at a center of mass distance of $r_{TP} = 0.38 \pm 0.01 \text{ nm}$, where significant repulsion takes place ($G \approx 5 \text{ kJ/mol} \approx 2 k_B T$, see panel B). As depicted in panel A (side view), θ_3 denotes the angle between the TMAO dipole vector and the z -axis (which is parallel to the stretched polyGLY chain) and θ_4

denotes the angle between the TMAO dipole vector and the normal vector of the plane defined by the z -axis and the center of mass of TMAO (see panel A, top view). The dashed black line in Figure 7E indicates distributions expected in the case of orientational isotropy. Both angles do not exhibit any pronounced maxima in their distribution, suggesting the absence of preferred TMAO angular configurations which would lead to configurational entropic repulsion. Closer inspection of the angular distributions in dependence on the position along the peptide (see Supporting Information) is consistent with this conclusion. This result again underlines the subtlety of our dipolar/hydrophobic frustration mechanism, according to which hydrophobic groups of suitable size prevent the dipoles of interacting molecules from attaining favorable mutual configurations. The latter can be seen in Figure S8 of the Supporting Information, where the TMAO–polyGLY pair interaction in the absence of water is found to be much more favorable than in the presence of water.

CONCLUSIONS

A large class of naturally occurring stabilizing osmolytes consists of small, highly water-soluble molecules that combine a large molecular dipole moment with pronounced hydrophobicity in the form of methyl groups located around the positively charged end of the molecule. TMAO is one example; one other example is betaine, which results from the amino acid glycine by addition of three methyl groups to the N-terminus. The ubiquitous occurrence of these chemical structures, which we call dipolar/hydrophobic osmolytes (DHOs), suggests an underlying reason for combining hydrophobicity with dipolarity in one molecule. As the main result of our study, we find the antagonistic properties of dipoles and hydrophobic groups to be crucial for the efficient functioning of DHOs via the mechanism of dipolar/hydrophobic frustration: The dipoles, which are strongly hydrated by water layers, are hindered to electrostatically interact with other dipoles in a favorable fashion by the bulky hydrophobic groups centered around the positive end of the dipole; the hydrophobic groups on the other hand do not bind to other hydrophobic groups because of the considerable charge present within the hydrophobic domain. Although a DHO is both polar and hydrophobic, it can as a result of this frustration neither strongly bind to dipolar groups nor to hydrophobic groups. We note that the resulting repulsion between hydrated DHOs is different from steric repulsion, since it is enthalpy dominated.

The inability to bind to other molecules is key to an efficient stabilizing function: Since DHOs generally are repelled from many amino acids (tryptophan, among other amino acids, constitutes an exception which will be further explored by us in the future), the transfer free energy of amino acids into DHO solutions is positive and consequently the folded state of a protein is favored over the unfolded state. Since DHOs also repel each other in bulk solution, the nonideality parameter is positive and therefore the positive TFE is even more enhanced. It is this double effect of repulsion between DHOs themselves and between DHOs and peptides, both driven by essentially the same dipolar/hydrophobic frustration mechanism, that explains their widespread use in biology as well as their great potential for industrial applications. Our findings corroborate the importance of hydrophobic as well as dipolar contributions for the functioning of DHOs and in turn helps to rationalize the strong denaturing effect of a wide variety of different compounds that do not have the right proportion of

hydrophobicity and dipolarity, for example, urea or tetramethyl-urea.⁵⁸

We derive most of our insights into the DHO mechanism by looking at the properties of ff variants of TMAO, one of the most potent stabilizing osmolytes, which differ in their hydrophobicity and dipole strength from the optimal, realistic TMAO representation. Changing the molecular properties and considering unrealistic molecular species allows us to clearly see which properties are important for the behavior of the actual TMAO molecule and which are not. We think that this approach, which consists of global force-field variations around the optimal ff, will be useful for other situations as well. For example, DHOs typically have their hydrophobic groups centered around the positive charge; future work will tell whether this reflects the asymmetric acceptor/donor distribution on peptides, the water asymmetry, or whether this has no functional reason. Likewise, the above arguments explain why stabilizing osmolytes typically tend to be “super-stabilizing” due to nonlinear mixing effects that enhance the thermodynamic effect of a negative adsorption excess, $\bar{\Gamma} < 0$. One challenge for future work is to design “super-denaturants”, which would be characterized by a positive adsorption excess on the peptide surface, $\bar{\Gamma} > 0$, but at the same time should exhibit a positive nonideality parameter due to repulsive self-interactions in bulk, $f' > 0$.

ASSOCIATED CONTENT

S Supporting Information

Additional figures and tables on the concentration dependence of activity coefficients, on the parameters of the TMAO ff, on the density of TMAO solutions, on Kirkwood–Buff integrals, on the behavior of TMAO with sub-optimal parameterization, on TMAO–TMAO and TMAO–polyGLY interactions in vacuum, on the calculation of m -values, on the influence of the bond lengths on activity coefficients, on the position-dependence of the TMAO–polyGLY interaction, and on the bicubic interpolation are available free of charge via the Internet at <http://pubs.acs.org>.

AUTHOR INFORMATION

Corresponding Author

*E-mail: rnetz@physik.fu-berlin.de.

Present Address

^{II}E.S.: Institut Laue-Langevin, 6 rue Jules Horowitz, 38042 Grenoble, France.

Notes

The authors declare no competing financial interest.

ACKNOWLEDGMENTS

Financial support from the DFG (cooperative research group SFB 765) is gratefully acknowledged. The authors thank Felix Sedlmeier for insightful comments and the Leibniz Rechenzentrum München (LRZ projects pr28xe and pr63ca) and the computing cluster of Institut Laue-Langevin for computing time. E.S. acknowledges support from a Marie Curie Intra-European Fellowship within the European Commission 7th Framework Program.

REFERENCES

- (1) Arakawa, T.; Timasheff, S. N. The Stabilization of Proteins by Osmolytes. *Biophys. J.* 1985, 47, 411–414.

- (2) Brown, A. D.; Simpson, J. R. Water Relations of Sugar-Tolerant Yeasts: The Role of Intracellular Polyols. *J. Gen. Microbiol.* **1972**, *72*, 589–591.
- (3) Somero, G. N. From Dogfish to Dogs: Trimethylamines Protect Proteins from Urea. *Physiology* **1986**, *1*, 9–12.
- (4) Yancey, P. H.; Clark, M. E.; Hand, S. C.; Bowlus, R. D.; Somero, G. N. Living with Water Stress, Evolution of Osmolyte Systems. *Science* **1982**, *217*, 1214–1222.
- (5) Lippert, K.; Galinski, E. A. Enzyme Stabilization by Ectoine-Type Compatible Solute: Protection against Heating, Freezing, and Drying. *Appl. Microbiol. Biotechnol.* **1992**, *37*, 61–65.
- (6) Santoro, M. M.; Liu, Y.; Khan, S. M. A.; Hou, L.-X.; Bolen, D. W. Increased Thermal Stability of Proteins in the Presence of Naturally Occurring Osmolytes. *Biochemistry* **1992**, *31*, 5278–5283.
- (7) Lee, J. C.; Timasheff, S. N. The Stabilization of Proteins by Sucrose. *J. Biol. Chem.* **1981**, *256*, 7193–7201.
- (8) Tanford, C. Isothermal Unfolding of Globular Proteins in Aqueous Urea Solutions. *J. Am. Chem. Soc.* **1964**, *86*, 2050–2059.
- (9) O'Brien, E. P.; Ziv, G.; Haran, G.; Brooks, B. R.; Thirumalai, D. Effects of Denaturants and Osmolytes on Proteins Are Accurately Predicted by the Molecular Transfer Model. *Proc. Natl. Acad. Sci. U.S.A.* **2008**, *105*, 13403–13408.
- (10) Lin, T.-Y.; Timasheff, S. N. Why Do Some Organisms Use a Urea-Methylamine Mixture as Osmolyte? Thermodynamic Compensation of Urea and Trimethylamine N-Oxide Interactions with Protein. *Biochemistry* **1994**, *33*, 12695–12701.
- (11) Auton, M.; Bolen, D. W. Additive Transfer Free Energies of the Peptide Backbone Unit That Are Independent of the Model Compound and the Choice of Concentration Scale. *Biochemistry* **2004**, *43*, 1329–1342.
- (12) Hu, C. Y.; Kokubo, H.; Lynch, G. C.; Bolen, D. W.; Pettitt, B. M. Backbone Additivity in the Transfer Model of Protein Solvation. *Protein Sci.* **2010**, *19*, 1011–1022.
- (13) Greene, R. F., Jr.; Pace, C. N. Urea and Guanidine Hydrochloride Denaturation of Ribonuclease, Lysozyme, Alpha-Chymotrypsin, and Beta-Lactoglobulin. *J. Biol. Chem.* **1974**, *249*, 5388–5393.
- (14) Parsegian, V. A.; Rand, R. P.; Rau, D. C. Osmotic Stress, Crowding, Preferential Hydration, and Binding: A Comparison of Perspectives. *Proc. Natl. Acad. Sci. U.S.A.* **2000**, *97*, 3987–3992.
- (15) Athawale, M. V.; Dordick, J. S.; Garde, S. Osmolyte Trimethylamine-N-Oxide Does Not Affect the Strength of Hydrophobic Interactions: Origin of Osmolyte Compatibility. *Biophys. J.* **2004**, *89*, 858–866.
- (16) Bennion, B. J.; Daggett, V. Counteraction of Urea-Induced Protein Denaturation by Trimethylamine N-Oxide: A Chemical Chaperone at Atomic Resolution. *Proc. Natl. Acad. Sci. U.S.A.* **2004**, *101*, 6433–6438.
- (17) Cho, S. S.; Reddy, G.; Straub, J. E.; Thirumalai, D. Entropic Stabilization of Proteins by Tmao. *J. Phys. Chem. B* **2011**, *115*, 13401–13407.
- (18) Gilman-Politi, R.; Harries, D. Unraveling the Molecular Mechanism of Enthalpy Driven Peptide Folding by Polyol Osmolytes. *J. Chem. Theory Comput.* **2011**, *7*, 3816–3828.
- (19) Wei, H.; Fan, Y.; Gao, Y. Q. Effects of Urea, Tetramethyl Urea, and Trimethylamine N-Oxide on Aqueous Solution Structure and Solvation of Protein Backbones: A Molecular Dynamics Simulation Study. *J. Phys. Chem. B* **2010**, *114*, 557–568.
- (20) Zou, Q.; Bennion, B. J.; Daggett, V.; Murphy, K. P. The Molecular Mechanism of Stabilization of Proteins by Tmao and Its Ability to Counteract the Effects of Urea. *J. Am. Chem. Soc.* **2002**, *124*, 1192–1202.
- (21) Stumpe, M. C.; Grubmüller, H. Urea Impedes the Hydrophobic Collapse of Partially Unfolded Proteins. *Biophys. J.* **2009**, *96*, 3744–3752.
- (22) Xie, G.; Timasheff, S. N. The Thermodynamic Mechanism of Protein Stabilization by Trehalose. *Biophys. Chem.* **1997**, *64*, 25–43.
- (23) O'Connor, T. F.; Debenedetti, P. G.; Carbeck, J. D. Simultaneous Determination of Structural and Thermodynamic Effects of Carbohydrate Solutes on the Thermal Stability of Ribonuclease A. *J. Am. Chem. Soc.* **2004**, *126*, 11794–11795.
- (24) Politi, R.; Harries, D. Enthalpically Driven Peptide Stabilization by Protective Osmolytes. *Chem. Commun.* **2010**, *46*, 6449–6451.
- (25) Canchi, D. R.; Jayasimha, P.; Rau, D. C.; Makhatadze, G. I.; Garcia, A. E. Molecular Mechanism for the Preferential Exclusion of Tmao from Protein Surfaces. *J. Phys. Chem. B* **2012**, *116*, 12095–12104.
- (26) Street, T. O.; Bolen, D. W.; Rose, G. D. A Molecular Mechanism for Osmolyte-Induced Protein Stability. *Proc. Natl. Acad. Sci. U.S.A.* **2006**, *103*, 13997–14002.
- (27) Horinek, D.; Netz, R. R. Can Simulations Quantitatively Predict Peptide Transfer Free Energies to Urea Solutions? Thermodynamic Concepts and Force Field Limitations. *J. Phys. Chem. A* **2011**, *115*, 6125–6136.
- (28) Rösgen, J.; Pettitt, B. M.; Bolen, D. W. Uncovering the Basis for Nonideal Behavior of Biological Molecules. *Biochemistry* **2004**, *43*, 14472–14484.
- (29) Hess, B.; Kutzner, C.; van der Spoel, D.; Lindahl, E. Gromacs 4: Algorithms for Highly Efficient, Load-Balanced, and Scalable Molecular Simulation. *J. Chem. Theory Comput.* **2008**, *4*, 435.
- (30) Berendsen, H. J. C.; Grigera, J. R.; Straatsma, T. P. The Missing Term in Effective Pair Potentials. *J. Phys. Chem.* **1987**, *91*, 6269–6271.
- (31) Miyamoto, S.; Kollman, P. A. Settle: An Analytical Version of the Shake and Rattle Algorithms for Rigid Water Models. *J. Comput. Chem.* **1992**, *13*, 952–962.
- (32) Hess, B.; Bekker, H.; Berendsen, H. J. C.; Fraaije, J. G. E. M. Lincs: A Linear Constraint Solver for Molecular Simulations. *J. Comput. Chem.* **1997**, *18*, 1463.
- (33) Hoover, W. G. Canonical Dynamics: Equilibrium Phase-Space Distributions. *Phys. Rev. A* **1985**, *31*, 1695–1697.
- (34) Parrinello, M.; Rahman, A. Polymorphic Transitions in Single Crystals: A New Molecular Dynamics Method. *J. Appl. Phys.* **1981**, *52*, 7182.
- (35) Darden, T.; York, D.; Pedersen, L. Particle Mesh Ewald: An Nlog(N) Method for Ewald Sums in Large Systems. *J. Chem. Phys.* **1993**, *98*, 10089.
- (36) Essmann, U.; Perera, L.; Berkowitz, M. L.; Darden, T.; Lee, H.; Pedersen, L. G.; Smooth, A. Particle Mesh Ewald Method. *J. Chem. Phys.* **1995**, *103*, 8577.
- (37) Cornell, W. D.; Cieplak, P.; Bayly, C. I.; Gould, I. R.; Merz, K. M., Jr.; Ferguson, D. M.; Spellmeyer, D. C.; Fox, T.; Caldwell, J. W.; Kollman, P. A. A Second Generation Force Field for the Simulation of Proteins, Nucleic Acids, and Organic Molecules. *J. Am. Chem. Soc.* **1995**, *117*, 5179–5197.
- (38) Weerasinghe, S.; Smith, P. E. A Kirkwood–Buff Derived Force Field for Mixtures of Urea and Water. *J. Phys. Chem. B* **2003**, *107*, 3891–3898.
- (39) Besler, B. H.; Merz, K. M., Jr.; Kollman, P. A. Atomic Charges Derived from Semiempirical Methods. *J. Comput. Chem.* **1990**, *11*, 431–439.
- (40) Singh, U. C.; Kollman, P. A. An Approach to Computing Electrostatic Charges for Molecules. *J. Comput. Chem.* **1984**, *5*, 129–145.
- (41) Kast, K. M.; Brickmann, J.; Kast, S. M.; Berry, R. S. Binary Phases of Aliphatic N-Oxides and Water: Force Field Development and Molecular Dynamics Simulation. *J. Phys. Chem. A* **2003**, *107*, 5342–5351.
- (42) Hub, J. S.; de Groot, B. L.; van der Spoel, D. G_Wham - a Free Weighted Histogram Analysis Implementation Including Robust Error and Autocorrelation Estimates. *J. Chem. Theory Comput.* **2010**, *6*, 3713–3720.
- (43) Kirkwood, J. G.; Buff, F. P. The Statistical Mechanical Theory of Solutions. *I. J. Chem. Phys.* **1951**, *19*, 774–777.
- (44) Courtenay, E. S.; Capp, M. W.; Anderson, C. F.; Record, M. T., Jr. Vapor Pressure Osmometry Studies of Osmolyte–Protein Interactions: Implications for the Action of Osmoprotectants in Vivo and for the Interpretation of “Osmotic Stress” Experiments in Vitro. *Biochemistry* **2000**, *39*, 4455–4471.

- (45) Wang, A.; Bolen, D. W. A Naturally Occurring Protective System in Urea-Rich Cells: Mechanism of Osmolyte Protection of Proteins against Urea Denaturation. *Biochemistry* **1997**, *36*, 9101–9108.
- (46) *Handbook of Chemistry and Physics*; CRC: Boca Raton, FL, 1986.
- (47) Kozak, J. J.; Knight, W. S.; Kauzmann, W. Solute-Solute Interactions in Aqueous Solutions. *J. Chem. Phys.* **1968**, *48*, 675–686.
- (48) Macaskill, J. B.; Robinson, R. A.; Bates, R. G. Osmotic Coefficients and Activity Coefficients of Guanidinium Chloride in Concentrated Aqueous Solutions at 25°C. *J. Chem. Eng. Data* **1977**, *22*, 411–412.
- (49) Rösgen, J.; Pettitt, B. M.; Bolen, D. W. Protein Folding, Stability, and Solvation Structure in Osmolyte Solutions. *Biophys. J.* **2005**, *89*, 2988–2997.
- (50) Di Michele, A.; Freda, M.; Onori, G.; Paolantoni, M.; Santucci, A.; Sassi, P. Modulation of Hydrophobic Effect by Cosolutes. *J. Phys. Chem. B* **2006**, *110*, 21077–21085.
- (51) Garrod, J. E.; Herrington, T. M. Apparent Molar Volumes and Temperatures of Maximum Density of Dilute Aqueous Sucrose Solutions. *J. Phys. Chem.* **1970**, *74*, 363–370.
- (52) Tyrrell, W. J. V.; Kennerley, M. Viscosity B-Coefficients between 5° and 20° for Glycolamide, Glycine, and N-Methylated Glycines in Aqueous Solution. *J. Chem. Soc. A* **1968**, 2724–2728.
- (53) Tanford, C. *The Hydrophobic Effect: Formation of Micelles and Biological Membranes*; John Wiley: New York, 1973.
- (54) Pettitt, B. M.; Rossky, P. J. Alkali Halides in Water: Ion-Solvent Correlations and Ion-Ion Potentials of Mean Force at Infinite Dilution. *J. Chem. Phys.* **1986**, *84*, 5836–5844.
- (55) Sukenik, S.; Sapir, L.; Gilman-Politi, R.; Harries, D. Diversity in the Mechanisms of Cosolute Action on Biomolecular Processes. *Faraday Discuss.* **2013**, *160*, 225–237.
- (56) Tanford, C. Contribution of Hydrophobic Interactions to the Stability of the Globular Conformation of Proteins. *J. Am. Chem. Soc.* **1962**, *84*, 4240–4247.
- (57) Hu, C. Y.; Lynch, G. C.; Kokubo, H.; Pettitt, B. M. Trimethylamine N-Oxide Influence on the Backbone of Proteins: An Oligoglycine Model. *Proteins* **2009**, *78*, 695–704.
- (58) Pace, C. N.; Marshall, H. F., Jr. A Comparison of the Effectiveness of Protein Denaturants for B-Lactoglobulin and Ribonuclease. *Arch. Biochem. Biophys.* **1980**, *199*, 270–276.